Hindawi
Advances in Materials Science and Engineering
Volume 2022, Article ID 9431319, 16 pages
https://doi.org/10.1155/2022/9431319

Research Article

Experimental Study on the Property Degradation and Failure Mechanism of Weakly Cemented Sandstone under Dry-Wet Cycles

Zhaoyang Song,[1] **Lihui Sun**,[2] **Shouye Cheng**,[1] **Zhiqiang Liu**,[1] **Jie Tan**,[1] **and Fangbo Ning**[1]

[1]*Beijing China Coal Mine Engineering Company Limited, Beijing 100013, China*
[2]*School of Mining and Geomatics, Hebei University of Engineering, Handan, Hebei 056038, China*

Correspondence should be addressed to Lihui Sun; slh2002789@sina.com

Received 28 October 2021; Revised 14 December 2021; Accepted 22 December 2021; Published 18 January 2022

Academic Editor: José António Fonseca de Oliveira Correia

Taking the weakly cemented sandstone of Ordos, China, as the research object, the evolution law between the relative stress of weakly cemented sandstone and the multiparameters of the acoustic emission under different dry-wet cycles was explored, and the critical failure identification mode of weakly cemented sandstone under dry-wet cycle was established. The results show that as the number of dry-wet cycles increases, the wave velocity loss rate gradually increases. Overall, the longitudinal wave loss rate is larger than the shear wave loss rate, indicating that the longitudinal wave is more sensitive to the degradation of weakly cemented sandstone. With an increase in the number of dry-wet cycles, the crack is mainly caused by the main crack penetration failure, and the secondary crack is significantly reduced. The fractal dimension decreases with an increase in the dry-wet cycles and reaches its maximum at 0 dry-wet cycles, which means that 0 dry-wet cycles witness the most complex morphology of fractures within the weakly cemented sandstone. This finding indicates that the dry-wet cycle inhibits the generation and expansion of fractures. The event rate appears to be close to 0 before the rupture, and then the platform oscillates, followed by a sudden increase. The acoustic emission b value is relatively high during the initial stage and then decreases, which is the initial damage process. The elastoplastic phase rises again, the peak stage decreases rapidly, and the weakly cemented sandstone undergoes unstable damage. The change in the acoustic emission entropy value is exactly the opposite of the b value change law. When the weakly cemented sandstone reaches the critical failure state under different dry-wet cycles, the relative stress value is 95%. The test results provide new methods and a basis for the damage evolution mechanism and fracture prediction of weakly cemented sandstone under dry-wet cycles.

1. Introduction

In the western part of China, the coal mining areas represented by Erdos and Yulin have the characteristics of low strength, poor cementation, easy weathering, and water softening, expansion, or disintegration. Therefore, domestic scholars call it a weak cemented formation [1, 2]. In recent years, there have been many disasters, such as sand collapse, water inrush, and large bearing and impact pressures, during the deep mining of coal in the western region [3]. The special physical and mechanical properties of weakly cemented strata sandstones are the intrinsic factors leading to the above disasters [4]. At the same time, weakly cemented sandstone has a low degree of cementation and poor stability of the surrounding rock, which leads to severe deformation, long duration, and serious damage of the surrounding rock of the diverticulum (roadway) [5, 6]. When the traditional theory of anchor net spray technology is used for support, the anchoring phenomenon of the anchor rod and the anchor cable sometimes occurs, and the support effect is poor (or it is difficult to provide support). The interaction between water and rock is a complex physical and chemical process. Weakly cemented sandstone is more deteriorated under saturated conditions, and water is an important cause of the significant decrease in macroscopic mechanical properties and the deterioration of the microstructure [7]. Weakly cemented sandstone has a high content of cemented clay minerals, which can easily interact with water. Water molecules enter between the cell layer and the particle interface, forming interlayer expansion and interparticle

expansion, which destroys the complete structure of the weakly cemented sandstone [8]. In order to solve the problem of rock instability and destruction of underground reservoir in coal mine, CFD-DEM coupled simulation of broken rock mass movement during water seepage in an underground goaf reservoir was analyzed, and we investigated the effect of seepage on broken rock mass porosity under different stress states [9] . Therefore, underground structure construction is carried out in the weakly cemented stratum under the conditions of dry-wet circulation, and the surrounding rock mass of the project is more likely to cause instability and damage.

Aiming at the influence of dry-wet circulation on the degradation of the macroscopic mechanical properties of rock, some scholars have carried out experimental research on the influence of dry-wet circulation on the mechanical properties of different lithologies. Previous studies have shown that the interaction between water and rock causes irreversible progressive damage to the rock. As the number of dry-wet cycles (the period of water-rock action) increases, the degradation effect has a cumulative development trend [10]. Through 15 dry-wet cycle tests on the slightly weathered sandstone, it was found that the dry-wet cycle caused irreversible progressive damage to the rock specimen [11]. The elastic modulus, uniaxial and triaxle compressive strength, cohesion, internal friction angle, and other parameters of the red sandstone after 8 dry-wet cycles were reduced to varying degrees [12]. With an increase in the number of dry-wet cycles, the tensile strength and elastic modulus of the altered rock first decrease and then stabilize. Therefore, for rocks with special lithology, the attenuation of the rock strength after the dry-wet cycle does not increase with an increasing number of cycles, but there is a critical cycle [13, 14]. When considering the influence of the water pressure rise and fall and the influence of dry-wet circulation factors, the YRK-1 rock soaking instrument developed by a research and development method was used to study the deterioration law of sandstone, and the mechanical properties and deterioration mechanism of sandstone with only dry-wet circulation or saturation were significantly different [15]. To efficiently evaluate the reutilization of gangue wastes by gangue backfilling mining and its advantage in overburden aquifer protection, non-Darcy hydraulic properties and deformation behaviors of granular gangues were studied through laboratorial, theoretical, and in situ aspects. An improved Kruger model was established to predict the permeability evolution by the fractal dimension, and the improved Kruger model has better accuracy than the original one [16]. In addition, foreign scholars such as [17–20] and [21] conducted a series of experiments on the interaction between water and rock on sandstone, shale, mudstone, and other rock specimens. The effects of water on the physical and mechanical properties of rock and the degradation mechanism were studied.

The interaction between water and rock is essentially the result of a change in the rock microstructure system. Some scholars studied the mechanism of the disintegration and softening of mudstone, analyzed the changes in the material composition and microstructure before and after the softening of mudstone, obtained the change law of the microstructure during the interaction between water and mudstone, and studied the mechanism of microscopic degradation [22, 23]. Through the saturated water test on soft mudstones, such as sandy mudstones and argillaceous siltstones, the deterioration laws of the microstructure, ion concentration, and mechanical properties during the interaction between water and soft rock were studied [24]. The corresponding relationship between the number of acoustic emission events and crack expansion was investigated during the shear failure of rock specimens, under different conditions of a 0%, 50%, and 100% moisture content [25]. The evolution of the surface morphology of mudstone with the number of dry-wet cycles was obtained by means of x-ray diffraction and microscopy. A series of point-bending tests were conducted on granite disc samples by acoustic emission experiments, which shows that the height/diameter ratio determines the failure mode of granite samples [26].

In conclusion, through extensive research, scholars have acquired a certain understanding of the changes in fractures, pores, mechanics, and properties of other stones caused by dry-wet cycle damage. These results have provided an effective reference for the research of this paper. However, the weakly cemented sandstones in western China have a short diagenesis time and low maturity, and their microstructure and mineral compositions are quite different from those of other types of rocks. These factors inevitably lead to the physical-mechanical properties of weakly cemented sandstones under the action of dry-wet cycles being significantly different from those of other rocks [27].

Therefore, in this study, weakly cemented sandstones in western China were investigated. First, the macroscopic and mesoscopic degradation laws of weakly cemented sandstone under different dry-wet cycle conditions were studied by ultrasonic testing and quantitative evaluation of minerals by scanning electron microscopy (QEMSCAN) testing. Second, the uniaxial compression testing of weakly cemented sandstone under different conditions of dry-wet cycles was carried out, and acoustic emission detection measurements were performed simultaneously. The physical and mechanical properties of the weakly cemented sandstone under different dry-wet cycles were analyzed. The evolution law between the deformation and failure characteristics of weakly cemented sandstones and multipara meters of acoustic emission under different dry-wet cycles was studied. Finally, the critical failure identification mode of weakly cemented sandstone under dry-wet cycling conditions was established. The deterioration law and rupture precursor identification of weakly cemented sandstone in western China under different dry-wet cycles were studied. The results can reasonably guide the design and scientific evaluation of the stability of the surrounding rock.

2. Experimental Design

2.1. Specimen Preparation. The rock specimens used in the test were taken from the Hongqinghe coal mine in Ordos, Inner Mongolia Autonomous Region of China. Cretaceous coarse-grained sandstone was 380 m underground. The core

was sealed with plastic wrap, the core layer was clear, and there were no obvious cracks on the surface. The appearance of the rock specimen was dark purple and gray-purple. The main components of the specimen were quartz, albite, potassium, feldspar, illite, and chlorite. The fabrication of the specimens was in strict accordance with the standards of the International Society for Rock Mechanics. To be specific, the specimen was drilled in the parallel bedding direction, and the specimens were fabricated into Φ 50 mm × 100 mm cylinders whose two end faces were smoothed by a double-end face grinding machine. The processing accuracy met the standards that the non-parallelism error of both ends should be smaller than 0.05 mm, and the roughness error of each face should be smaller than 0.02 mm. For the remainder of the specimens, the sandstones were gently tapped with a hammer to break them into sandstone lumps with the length, width, and height of the lumps smaller than 10 mm. Sandstone lumps with smooth surfaces were selected for the QEMSCAN experiment. The physical parameters and composition analysis data of Cretaceous sandstone (−380 m) specimens are given in Table 1.

2.2. Experimental Equipment. Dry-wet cycle equipment: the drying box was an NMT-1007 single door test box produced by Beijing Nitrite Drying Technology Co., Ltd. The maximum operating temperature of the equipment was 250°C, and the intelligent temperature controller guaranteed temperature accuracy. Internal cleanliness can reach thousands of dust-free environments. The total power of the instrument was 6 kW. The saturation device is a glass container, and the saturated medium is distilled water.

Uniaxial compression experimental system: the experiment adopted a GAW-2000 rock rigid compression tester manufactured by Changchun Chaoyang Instrument Co. The system, which is composed of a press machine, a DCS controller, and a power test control program, boasts the functions of closed-loop control, constant load control, and load retention. Moreover, the system whose hydraulic oil pump can reach a maximum load of 2000 kN is able to realize equal loading, constant-rate loading, and force-displacement compound control.

Acoustic emission monitoring system: the acoustic emission monitoring system monitored and collected acoustic emission data during the process of uniaxial compression failure. Acoustic emission was adopted using the PCI-2 multichannel acoustic emission monitoring system produced by the PAC of American Physical Acoustics Company. The rock mechanics and acoustic emission testing systems are shown in Figure 1.

Quantitative evaluation of minerals by scanning electron microscopy (QEMSCAN): this technique can be used for the quantitative evaluation of minerals. The complete system included an electronic scanning microscope with a specimen chamber, four x-ray energy spectrometers, and special software (I Discover) that automatically acquired, analyzed, and processed the data. The surface of a specimen can be scanned with a high-energy electron beam accelerated along a preset raster scanning mode, and a color map of the embedded characteristics of mineral aggregates can be obtained.

Ultrasonic measurement system: the instrument for measuring the acoustic parameters of weakly consolidated sandstone after dry-wet cycling was an NM-4A nonmetallic ultrasonic testing analyzer produced by Beijing Kangkerui Engineering Testing Technology Co. The system emits a voltage range of 60 V to 1000 V, a sampling period of 0.05 μs to 6.4 μs, and an amplifier bandwidth of 5 Hz to 500 kHz. There are 2 receiving channels for testing the wave velocity of the longitudinal and transverse waves of rock specimens.

2.3. Experimental Procedures

2.3.1. Dry-Wet Cycle Treatment. The prepared standard rock specimens were dried in an oven. The temperature was 105°C, and the time was 24 h. After cooling, the specimens were vacuumed. The free water absorption method was used to saturate the rock specimens. First, the water was injected to 1/3 of the height of the specimen and then to 2/3 of the height of the specimen after 12 h. After that, the water was injected to all heights of the specimen, and the specimen was soaked in distilled water for another 24 h. Then, the rock specimen was placed in a 105°C drying box for 24 h. The above steps were followed for one dry-wet cycle. Each type of specimens was divided into 3 groups. Each group was composed of 3 specimens, with one group reserved for standby application. The groups were applied to mechanical tests with the dry-wet circle, $n = 0$, 5, and 10 (n is the number of wet dry cycles). The groups were applied to physical parameter tests with the dry-wet circle $n = 0, 1, 2, \ldots$, and 10 in the distilled water environment.

2.3.2. Compression experiment. The uniaxial compression test was used as deformation control. To ensure that the rock specimen was in full contact with the loading surface, the contact noise generated during contact was prevented from affecting the acoustic emission monitoring result, first loaded to 1.5 kN, and then loaded at a rate of 0.006 mm/min until destruction. In synchronization, an acoustic emission monitoring system was adopted to carry out the synchronous monitoring of the specimen failure process. To eliminate the influence of environmental noise on the acoustic emission monitoring data, in the test, the preamplifier gain was 40 dB, the threshold value was 40 dB, the waveform sampling frequency was 1 MSPS, the retrigger was 256, and the length was 2 K. The acoustic emission sensor selected was an R6 resonant-type high sensitivity sensor with a resonant frequency of 35~100 kHz. In the experiment, Vaseline was applied between the sensor and rock specimen to enhance the coupling between them and reduce the attenuation of the acoustic emission signal to ensure the strict correspondence between the mechanical test and acoustic emission

Table 1: Physical parameters and composition analyses of Cretaceous sandstone (−380 m) specimens in this study.

Sampling site	Physical parameter				Composition analysis			
	Longitudinal wave velocity (mm/μs)	Density (g/cm^3)	Porosity (%)	Water absorption (%)	Quartz content (%)	Albite content (%)	K-feldspar (%)	Chlorite (%)
Cretaceous sandstone (−380 m)	25.03	2.46	4.32	1.78	34.56	22.49	12.32	7.64

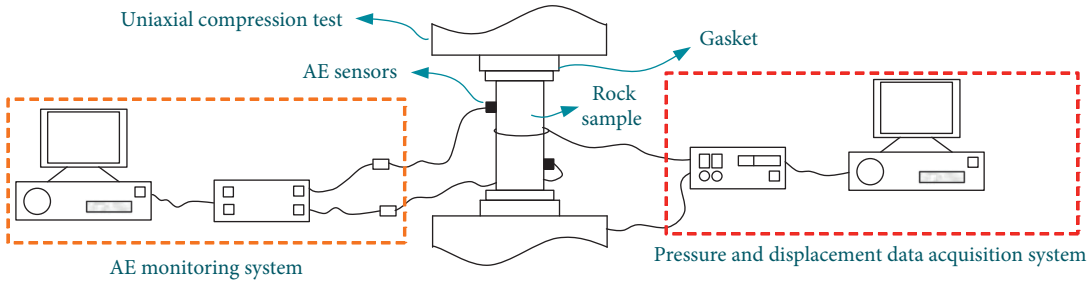

Figure 1: Schematic diagram of the experimental instrument.

monitoring data in terms of time; the test data acquisition system was synchronized and timed before the start of the test.

2.3.3. QEMSCAN Experiment. To obtain good images and mineral content data, each specimen was coated with a film for improving the conductivity. The specimen was placed in the QEMSCAN observation room and vacuumed for 10 min, and then its height and inclination were adjusted to make it stay in the appropriate position. A random part of the specimen was selected to be magnified and scanned, and the corresponding QEMSCAN images and mineral content data were obtained.

3. Microstructure Characteristics of the Damage and Rupture of Weakly Cemented Sandstone under Different Numbers of Dry-Wet Cycles

3.1. Qualitative Analysis of Fracture Evolution Observed in the QEMSCAN Images. The weakly cemented sandstone specimens treated under different dry-wet cycles were observed via QEMSCAN, and the results are presented in Figure 2. As seen from the experimental results, the weakly cemented sandstone specimens show obvious fracture characteristics in the QEMSCAN images under different numbers of dry-wet cycles, which can reflect the microstructure characteristics of the fracture evolution of the weakly cemented sandstone during the damage process.

It can be seen from Figure 2 that, with the number of dry-wet cycles, the number of fractures grows. With an increase in the dry-wet cycle, the microstructure of weakly cemented sandstone becomes looser. New fractures occur mainly in the intergranular cementing material.

First, the dissolution corrosion of the particles themselves causes the boundaries to be blurred and the skeleton particles to become looser. Second, water molecules enter the intergranular pores, and the dissolution of the pore materials leads to an increase in pores. The connectivity between the macrospores improves, and water molecules are more likely to enter the fine pores, resulting in an increase in microcracks. As the number of dry-wet cycles increases, the pore distribution tends to be uniform, and the cemented material exhibits certain curling, muddy, broken, and porous characteristics. These characteristics result in a cohesive force of the rock, a decrease in the internal friction angle, and a decrease in the mechanical strength.

According to the comprehensive analysis, during the dry-wet cycle, the cemented material between the weakly cemented sandstone particles is first destroyed. As the number of dry-wet cycles increases, the connectivity between the particles improves, and the friction between the particles decreases. As shown in Figure 2, the crack path extends mainly along the grain boundaries and occurs in the cementitious material. After the dry-wet cycle, the degree of the disturbance sensitivity is reduced due to the weakening of the cemented material. Therefore, for weakly cemented sandstones, the mechanical properties of cemented materials are the key factors affecting the physical and mechanical properties of weakly cemented sandstones.

3.2. Quantitative Analysis of the Mineral Content Parameters. QEMSCAN was used to test the percentage of the mineral content of weakly cemented sandstone under different cycles of dry-wet cycles, and quantitative test results were obtained, as shown in Figure 3. As the number of dry-wet cycles increases, the mineral content of weakly cemented sandstones changes significantly.

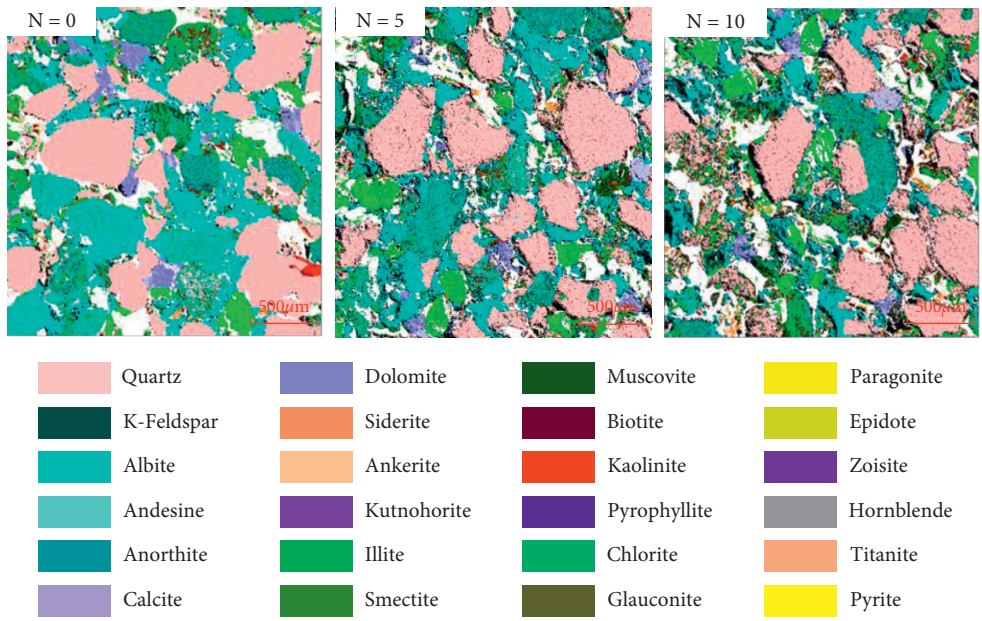

Figure 2: QEMSCAN images of weakly cemented sandstone under different numbers of dry-wet cycles.

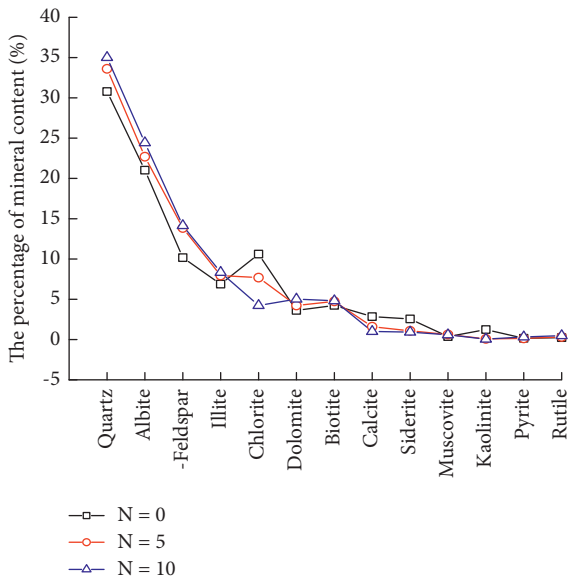

Figure 3: Percent change in the mineral content of weakly cemented sandstone under different numbers of dry-wet cycles.

With the increase in the number of dry-wet cycles, the content of minerals such as quartz and mica in weakly cemented sandstone increased, and the content of minerals such as potassium feldspar, albite, and illite decreased. The main reason for this change is that some mineral particles in the weakly cemented sandstone process cause mineral dissolution under the action of water, causing the mineral to dissolve. Therefore, during the interaction between water and rock, the mineral content dissolved in water is reduced, resulting in a corresponding increase in the proportion of water-insoluble minerals. As the number of dry-wet cycles increases, the reduction of minerals dissolved in water leads to the destruction of the mineral aggregates that constitute the mesostructured, which in turn leads to the structural damage and reduced strength of the weakly cemented sandstone.

During the interaction between the minerals and water of the weakly cemented sandstone, mineral dissolution, and secondary damage, the cement material between the particles is destroyed, causing water molecules to enter between the particles. The cemented material between the particles and the mineral particles themselves undergo physical and chemical reactions, which generate a large amount of micropores and a local stress concentration on the microstructure, causing the particulate matter constituting the skeleton structure to peel off and the internal structural system to be destroyed. These effects eventually lead to changes in the macroscopic physical and mechanical properties of weakly cemented sandstones.

4. Mechanical Properties of Weakly Cemented Sandstone under Different Times of Dry-Wet Cycle

4.1. Analysis of Physical Parameters. The changes in the mass, volume, and wave speed of the weakly cemented sandstone specimen under different times of dry-wet cycles were measured by an electronic balance, a Vernier caliper, and ultrasonic equipment. To intuitively describe the degradation law of weakly consolidated sandstone under different dry-wet cycles, the loss rate S is introduced to reasonably describe the variation law of weakly cemented sandstone specimens during the cycle:

$$S = \left(\frac{S_N}{S_O} - 1\right) \times 100\%, \quad (1)$$

where S_N is the parameter of the specimen after N cycles and S_O is the parameter of the initial state of the specimen.

As shown in Figure 4, a series of changes in the physical state occur after the weakly cemented sandstone specimen is subjected to different times of the dry-wet cycles. It can be seen from Figure 4 that as the number of cycles increases, the mass loss rate of the specimen increases first and then decreases. After the first to fourth cycles, the mass increases, the water absorption is greater than the loss of the rock components, but it is not damaged; the mass of the fifth cycle begins to decrease significantly, and the water remains in a stable state during the soaking-drying cycle. At this level, with an increase in the number of cycles, some rock minerals begin to loosen, and the quality begins to decrease. After the 8th cycle, the mass loss becomes faster due to the cumulative effect of multiple cycles. As shown in Figure 4, the volume of the weakly cemented sandstone specimen after each dry-wet cycle is measured using a Vernier caliper. As the number of dry-wet cycles increases, the volume of weakly cemented sandstone does not change significantly.

As shown in Figure 5, as the number of dry-wet cycles increases, the wave velocity loss rate gradually increases. Due to the cumulative effect of multiple cycles, the wave speeds of the longitudinal and transverse waves are significantly reduced after the fifth cycle. Then, the shear wave velocity changes slow down, and the curve slows down, but the overall trend shows a downward trend. After the 8^{th} cycle of the longitudinal wave velocity, the longitudinal wave velocity is again greatly reduced, and thereafter, the wave velocity loss rate is slowed down. Overall, the longitudinal wave loss rate is larger than the shear wave loss rate, indicating that the longitudinal wave is more sensitive to the degradation of weakly cemented sandstone.

4.2. Analysis of the Deformation Characteristics. Under uniaxial compression conditions, the variation in the axial stress-strain curve of a weakly cemented sandstone specimen is roughly divided into the following four stages [28]: pore and fracture compression and compacting stage, microfracture unsteady development stage (linear elastic deformation stage), fracture unsteady growth stage (progressive rupture stage), and post-rupture stage. Figure 6(a) shows the stress-strain curves of weakly cemented sandstone specimens treated for different numbers of dry-wet cycles. According to the test results in Figure 6(a), the stress-strain changes in the weakly cemented sandstone specimens treated under different times of dry-wet cycles are analyzed as follows.

The strains of the weakly cemented sandstone specimens in the compression and compacting stage are significantly greater than those in low-number cycles, and the strains grow with increasing cycles. The effect of water is large in this stage because the effect of water loosens the specimen structure, increases the internal fractures, and improves the porosity, thus prolonging the compression and compacting stage. Meanwhile, due to the softening effect of water on the clay cement, the cement material between some particles is also compressed.

In the microfracture unsteady development stage, the strains of the weakly cemented sandstone specimens are small under different numbers of dry-wet cycles. Under different numbers of dry-wet cycles, the stress-strain curves are dominated by the unsteady fracture growth stage, and the curves bend downward before the peak stresses are reached. At 0 and 5 dry-wet cycles, before the peak stresses are reached, the stress-strain curves are almost straight with no obvious bending stage before rupture. Under the action of 10 dry-wet cycles, obvious ductile failure characteristics appear at this stage.

As can be observed from the post-rupture stage, the failure modes of the weakly cemented sandstone specimens can be classified into two types, namely, brittle failure and ductile failure. At 0 and 5 dry-wet cycles, the specimens are subjected to brittle failure. That is, in this range, after the peak stresses are reached, the stresses drop rapidly, while the strains change slightly. At 10 dry-wet cycles, the weakly cemented sandstone specimens are subjected to ductile

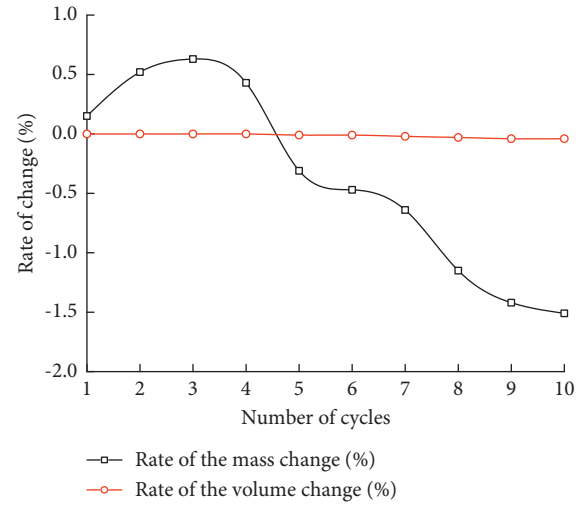

Figure 4: Variation curves of the physical parameters of weakly cemented sandstone under different numbers of dry-wet cycles.

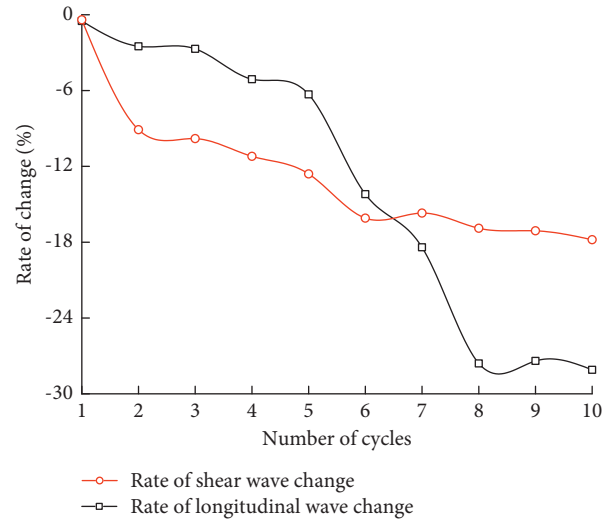

Figure 5: Loss rate curves of the wave velocity of weakly cemented sandstone under different numbers of dry-wet cycles.

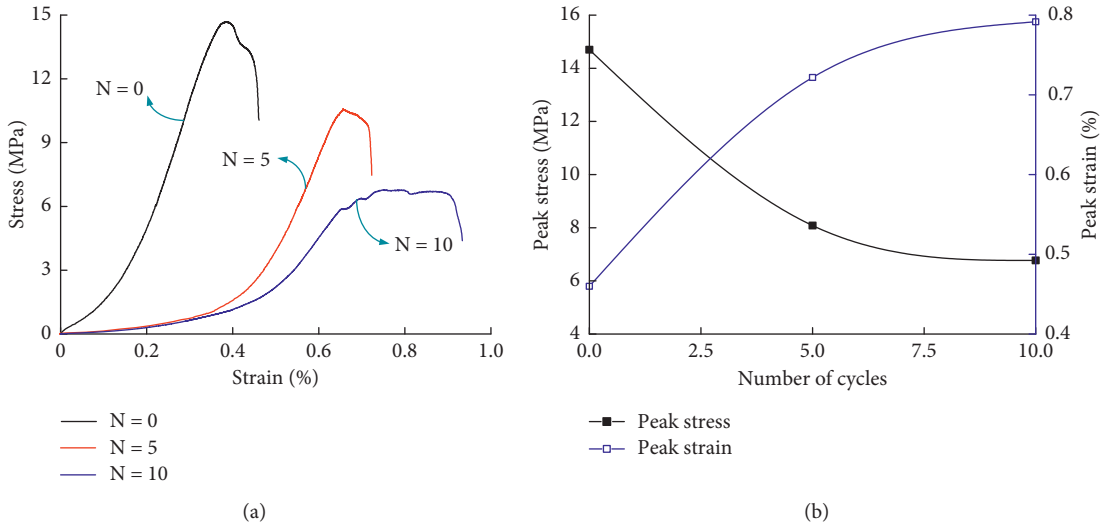

Figure 6: Uniaxial stress-strain curves of the WCST specimens under different numbers of dry-wet cycles. (a) Stress-strain curves. (b) Peak stress and peak strain.

failure. That is, after the peak stresses are reached, the stresses decline gradually rather than drop rapidly with increasing strain.

It can be seen from the analysis of Figure 6(b) that the peak value of the average compressive strength of the weakly cemented sandstone decreases with increasing number of dry-wet cycles, and the peak intensity of the rock decreases by approximately 41.3% after 5 dry-wet cycles. The peak intensity reduction after 10 dry-wet cycles is approximately 62.1%. With an increase in the number of dry-wet cycles, the axial strain increases when the weakly cemented sandstone reaches the peak strength. The main reason for this increase is that as the number of dry-wet cycles increases, the softening effect of the cemented material in the weakly cemented sandstone is obvious, and the ability of the weakly cemented sandstone specimens to resist plastic deformation is enhanced.

4.3. Qualitative Analysis of the Macroscopic Fracture Evolution. The fractured weakly cemented sandstone specimens were photographed from three different angles, and an expanded image was obtained. To make the cracks in the photos clearer and easier to observe, the shooting results were further sketched using Photoshop CS6 graphics processing software. Figure 7 shows the diagram of the macroscopic failure characteristic variation in the weakly cemented sandstone specimens with an increase in the number of dry-wet cycles. It can be observed from Figure 7 that after the weakly cemented sandstone undergoes water-rock interaction under different dry-wet cycles, the main fracturing surfaces of the weakly cemented sandstone specimens are parallel to the axial direction, and most of the cracks are vertically distributed. As the number of dry-wet cycles increases, both the number of cracks and the degree of coal fragmentation decrease, which indicates that the end effect of the indenter is relatively weak in the experimental process.

It can be seen from Figure 7 that, after 0 dry-wet cycles, the rock specimens undergo columnar splitting failure with many broken sandstone particles, there are fracture zones on both sides of the main crack, and there are a large number of secondary cracks. Meanwhile, there is V-shaped damage in a small local area, the degree of fracture is relatively serious, and the stress disturbance is obvious. After 5 dry-wet cycles, the rock specimens undergo columnar splitting failure with small broken sandstone particles and an obvious transverse crack, producing two small shear surfaces (one at the top and the other at the bottom) and many broken coal particles. After 10 dry-wet cycles, the specimens experience both columnar splitting failure and shear failure, and the secondary cracks are significantly reduced.

In summary, as the number of dry-wet cycles increases, the failure mode of the weakly cemented sandstone specimens changes from splitting failure to splitting-tensile combined failure and shear-tensile combined failure, and the secondary cracks are significantly reduced. This behavior is due to the relative smoothing of the fracture surface caused by the softening and muddy action of water on the cemented material inside the weakly cemented sandstone. Therefore, the dry-wet cycle causes the disturbance sensitivity of the weakly cemented sandstone to decrease and the degree of fracture to be weakened.

4.4. Quantitative Analysis of the Macroscopic Fracture Evolution. Through programming via MATLAB, macroscopic failure images of the weakly cemented sandstone specimens treated under different numbers of dry-wet cycles were processed. The corresponding binary images are exhibited in Figure 8. Through the feature extraction of the binary images and the refined binary images, the basic characteristic parameters (fracture rate, fracture number, and average fracture width) of weakly cemented sandstone specimen fractures under different numbers of dry-wet cycles can be calculated and analyzed. The results are presented in Figure 9.

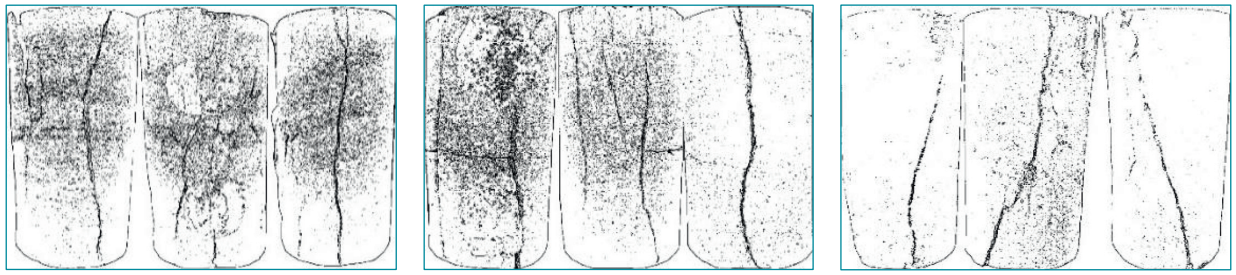

(a) (b) (c)

Figure 7: Macroscopic failure characteristics of the WCST specimens under different numbers of dry-wet cycles. (a) $N = 0$. (b) $N = 5$. (c) $N = 10$.

(a) (b) (c)

Figure 8: Binary images of WCST specimens under different numbers of dry-wet cycles. (a) $N = 0$ (b) $N = 5$. (c) $N = 10$.

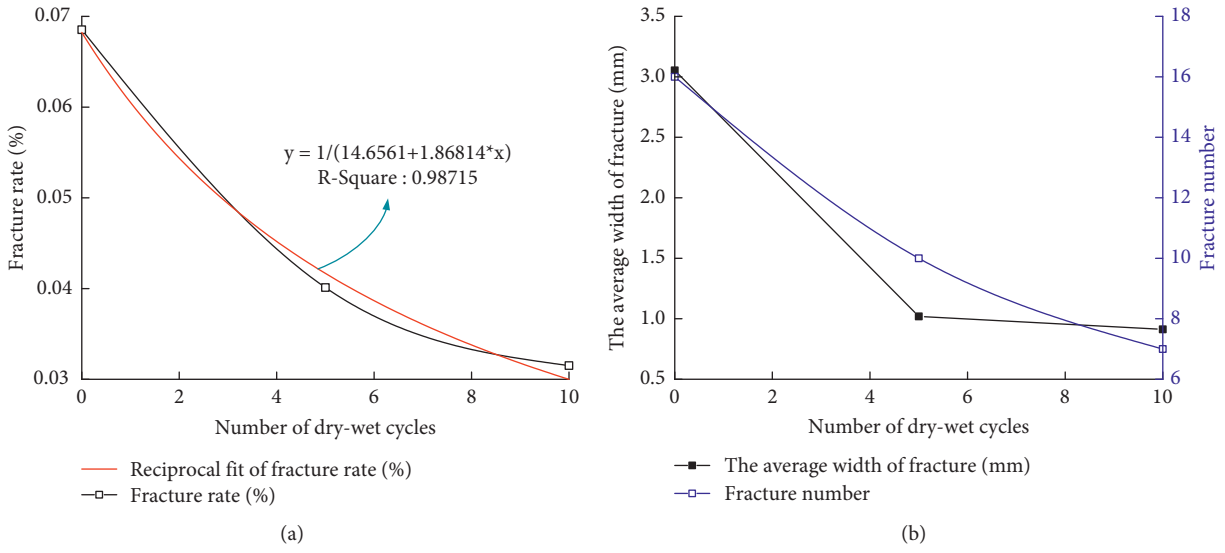

(a) (b)

Figure 9: Change curves of the weakly cemented sandstone specimen fracture parameters with different numbers of dry-wet cycles. (a) Fracture rate. (b) Fracture width and number.

As shown in Figure 9(a), as the number of dry-wet cycles rises, the fracture rate of the weakly cemented sandstone specimens decreases. With the number of dry-wet cycles from 0 to 5 to 10, the fracture rate changes from 0.068% to 0.04% to 0.031%, respectively. As shown in Figure 9(b), with the rise of the number of dry-wet cycles, the average fracture width and fracture number of the weakly cemented sandstone specimens also show a downward trend overall. This phenomenon is caused by two factors. One is that the water dissolves some of the minerals in the weakly cemented sandstone under the action of dry-wet cycles, resulting in poor cementation performance between the particles. The other is that the process of water-rock interaction softens the existing particles and cement, resulting in a decrease in the stiffness of the microstructure system of the particles and the cement.

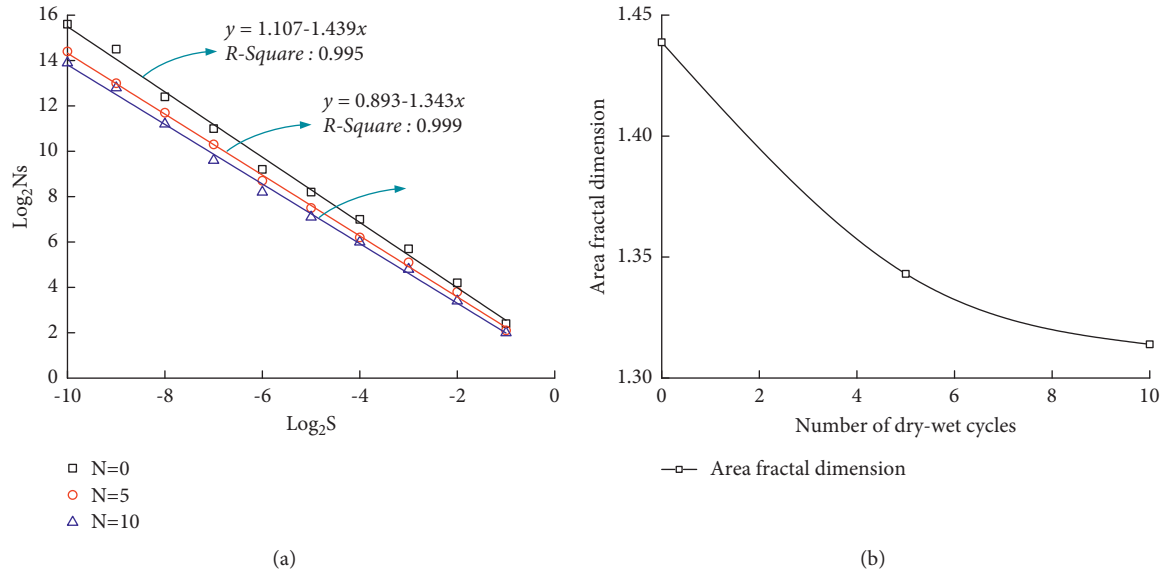

Figure 10: Change curves of the fractal dimension of the weakly cemented sandstone fracture area with different numbers of dry-wet cycles. (a) Fitting curves. (b) Fractal dimension.

4.5. Fractal Characteristics of the Fractures. Rock fractures have good fractal characteristics, and the fractal dimension of the fracture structure can quantitatively describe its complexity [29, 30]. In this paper, aiming at performing an in-depth analysis and study of fracture data, the fractal characteristics of the fracture data were described using the fractal dimension calculation model of the fracture distribution to further analyze and study the characteristics of weakly cemented sandstone specimen fracture structures [31–33].

The box dimension is the most widely used dimension. Let F be an arbitrary nonempty bounded subset of Space R^n [34]. For any $\delta > 0$, $N_r(F)$ is the minimum number of n-dimensional cubes (with a side length of δ) required to cover F. If d exists, when $\delta \longrightarrow 0$,

$$N_r(F) \infty \frac{1}{\delta^d}. \tag{2}$$

Then, F is the box dimension of d. In this case, there is only one positive number s, so

$$s = \lim_{\delta \longrightarrow 0} \frac{N_\delta(F)}{1/\delta^d}. \tag{3}$$

By taking the logarithm of both sides, the following equation can be obtained:

$$\begin{aligned} d &= \lim_{\delta \longrightarrow 0} \frac{\lg s - \lg N_\delta(F)}{\lg \delta} \\ &= -\lim_{\delta \longrightarrow 0} \frac{\lg N_\delta(F)}{\lg \delta}. \end{aligned} \tag{4}$$

According to the obtained binary images (Figure 8), the fractal dimension of the coal fracture area was calculated by using the "box method" algorithm in MATLAB software. The data points $\log_2 s$ and $\log_2 N_s$ were fitted, as shown in Figure 10(a). The fractal dimension of the weakly cemented sandstone fracture area is shown in Figure 10(b).

Figure 10(a) shows that a good linear relationship exists between the $\log_2 s$ and $\log_2 N_s$ of each weakly cemented sandstone specimen, and the absolute values of the slopes of the straight lines all lie between 1.43 and 1.31, which corresponds to the fractal dimension of the fracture area after different numbers of dry-wet cycle treatments. Thus, in the dry-wet cycle's range of 0~10, the distribution of fractures within the weakly cemented sandstone shows an obvious characteristic of self-similarity. Figure 10(b) shows that the fractal dimension decreases with the rise of dry-wet cycles and reaches its maximum at 0 dry-wet cycles. This finding means that the 0 dry-wet cycles witness the most complex morphology of fractures within the weakly cemented sandstone, which indicates that the dry-wet cycle inhibits the generation and expansion of fractures.

5. Acoustic Emission Parametric Characteristics of Weakly Cemented Sandstone Specimens under Different Numbers of Dry-Wet Cycles

Weakly cemented sandstone under different dry-wet cycles releases the acoustic emission signal during the deformation and failure process. These acoustic emission signals contain information on the critical damage of the weakly cemented sandstones. Therefore, to accurately identify the critical characteristics of weakly cemented sandstone before failure, a critical damage identification mode is established by analyzing the acoustic emission data. In this paper, the concept of the relative stress is introduced, which is defined as the ratio of the stress value to the peak stress at a point before the peak, expressed as a percentage. Therefore,

$$D_r = \frac{\sigma_i}{\sigma_{\max}} \times 100\%, \quad (5)$$

where D_r is the relative stress; σ_i is the stress value at a point before the peak stress; and $\sigma_{\max}$ is the peak stress.

5.1. Analysis of the Acoustic Emission Count Rate Parameters. The corresponding curves between the relative stress of the weakly cemented sandstone and the acoustic emission count rate under different conditions of dry-wet cycles were obtained. The result is shown in Figure 11. As shown in Figure 11, the acoustic emission count rate shows the same evolution trend in the weakly cemented sandstone under different dry-wet cycles. The level of acoustic emission is low during the initial stage, and the counting rate of acoustic emission events is gradually active when entering the plastic stage. However, when the weakly cemented sandstone reaches a relative stress of approximately 95%, the acoustic emission count rate drops sharply, and then a short adjustment occurs. After the peak intensity, the acoustic emission test piece count rate increases rapidly.

As shown in Figure 12, as the number of dry-wet cycles increases, the overall rate of sound emission events gradually decreases. After 5 dry-wet cycles, the corresponding acoustic emission event count rate decreased by 61.36%, and the corresponding acoustic emission event count rate decreased by 93.18% after 10 dry-wet cycles. This result is mainly due to the weak cementation of the weakly cemented sandstone between the argillaceous cement particles on the microstructure under the action of dry-wet circulation, resulting in a decrease in the internal friction angle and cohesion. Second, with the number of dry-wet cycles increasing, the overall amount of acoustic emission events is also reduced, indicating that as the number of dry-wet cycles increases, the softening of the cemented material between the particles is more pronounced, and the plastic deformation of the rock specimen increases.

5.2. Characteristics of the Acoustic Emission b Value of Weakly Cemented Sandstone under Dry-Wet Cycle. Acoustic emission is a sound wave phenomenon detected by strain energy release during rock deformation and destruction. In this paper, the acoustic emission is identified as a kind of microseismic activity. The characteristics of the weakly cemented sandstone deformation and failure processes under different numbers of dry-wet cycles are analyzed by the b value of the earthquake magnitude and frequency. The statistical relationship between the earthquake magnitude and frequency, proposed by B. Gutenberg and C.F. Richter in 1941 [35], was used. The famous G-R relationship is as follows:

$$\log N = a - bM, \quad (6)$$

where M is the magnitude, N is the magnitude of the magnitude, and a and b are constants.

The b value is a function of the relative magnitude distribution of the earthquake and is an important parameter for measuring the level of seismic activity. This value represents a function of the crack propagation scale. The corresponding change relationship between this value and the loading stress has important physical significance for analyzing the crack propagation, expansion, and destruction of rock specimens. Calculating the acoustic emission b value first determines the magnitude of the acoustic emission from rock specimen. This paper uses equation (6) to determine the magnitude.

$$M = \lg Q_i, \quad (7)$$

where Q_i is the acoustic emission energy.

In this paper, the acoustic emission b value of rock specimens is calculated by the least squares' method. To avoid too few acoustic emission events in a certain period, the calculation error of the b value is too large. According to the sampling frequency of the acoustic emission test, 1000 acoustic emission data points are taken as a calculation period. The frequency of the acoustic emission event and the average energy value representing the magnitude for a certain period are obtained. The statistical value of the acoustic emission b value is calculated as [36]

$$b = \frac{\sum M_i \sum \lg N_i - \Delta m \sum M_i \sum \lg N_i}{\Delta m \sum M_i^2 - \left(\sum M_i\right)^2}, \quad (8)$$

where Δm is the magnitude of the gear division with a value of 0.5 and M_i is the number of acoustic emission events at a certain stage.

According to the above calculation method, the variation in the acoustic emission b value during the uniaxial compression failure of weakly cemented sandstone under different dry-wet cycles is obtained. The calculation results are shown in Figure 13. Before the peak stress is reached, the b value of the acoustic emission constantly fluctuates during the stress loading process.

As shown in Figure 13, when the dry-wet cycle is applied 0 times, the b value of the acoustic emission appears to fluctuate slightly during the initial stage of loading. In this stage, the interior of the rock is mainly compacted, and the crack inside the rock develops slowly. After the end of the elastic phase and the transition to the plastic phase, the b value of the weakly cemented sandstone increases. Because of the poor cementation ability of weakly cemented sandstones, the crack propagation inside the rock mainly extends along the interface of the granular rubber, and many particles on the shear surface peel off, the proportion of small-scale damage increases, and the stress disturbance is sensitive. Before the stress reaches the peak value, the acoustic emission b value appears to be a short-term steady state, and its value is approximately 0.5. With a further increase in stress, when the rock specimen reaches the stress peak, the number of large cracks increases, and the b value of the acoustic emission drops sharply.

Under the condition of 5 cycles of dry-wet cycle, the b value of the acoustic emission is higher during the initial encryption stage. As the stress increases, the b value fluctuates, and the crack inside the rock develops slowly, causing it to be asymptotically destroyed. After entering the plastic state, the b value of the acoustic emission increases,

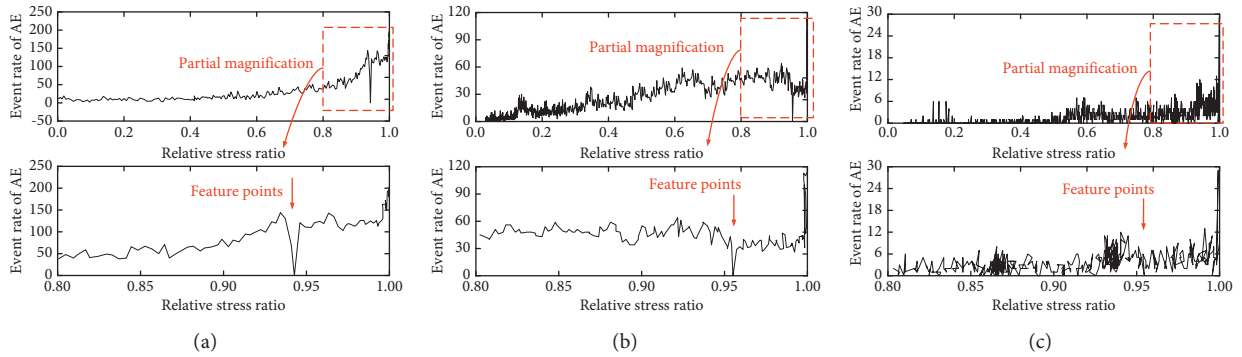

Figure 11: AE event counting rate of weakly cemented sandstone failure under different dry-wet cycles. (a) $N = 0$. (b) $N = 5$. (c) $N = 10$.

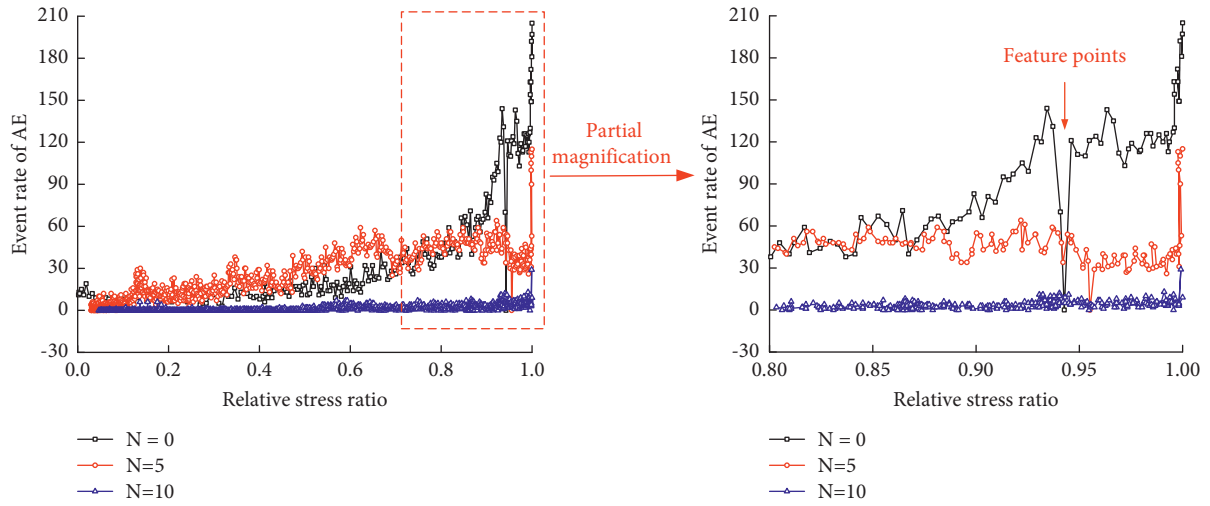

Figure 12: The overall quantity change in the number of acoustic emission events during the failure of weakly cemented sandstone under different dry-wet cycles.

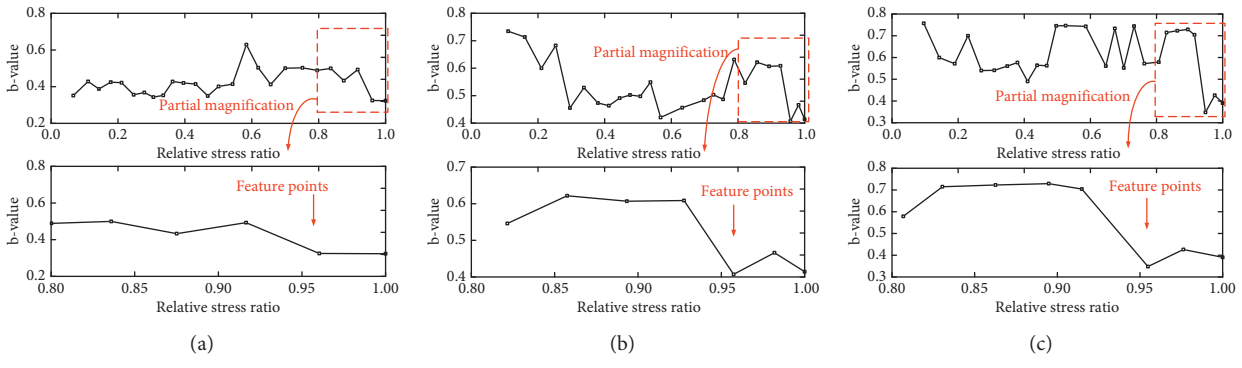

Figure 13: The variation rule of the acoustic emission b value during the process of weakly cemented sandstone failure under different dry-wet cycles. (a) $N = 0$. (b) $N = 5$. (c) $N = 10$.

indicating that the softening effect of water leads to the destruction of rock specimens mainly by small-scale damage, and the internal cracks of rock specimens are diffusely distributed. Before the stress reaches the peak value, the b value of the acoustic emission appears to decrease rapidly after the transient plate appears, indicating that the internal crack of the rock exhibits an unstable expansion state.

Comparing the conditions of 10 dry-wet cycles, the b value of the acoustic emission during the initial encryption stage is also high. As the stress increases, the b value fluctuates, and the internal crack of the rock develops slowly, mainly with asymptotic damage. After entering the plastic stage, the b value of the acoustic emission is in a fluctuating state, but it is still maintained at a high level, indicating that

the internal crack of the rock specimen is mainly caused by small-scale damage due to the softening effect of water, and the crack spreads and expands. The rock specimen destruction is dominated by ductile damage. When the peak stress is reached, the acoustic emission b value falls, and the main crack inside the rock forms and penetrates.

As shown in Figure 14, under different dry-wet cycles, the development state of the weakly cemented sandstone cracks can be reflected by the overall magnitude and trend of the acoustic emission b value. The weakly cemented sandstones after 0, 5, and 10 dry-wet cycles have similar acoustic emission b value changes before peak stress. When the relative stress is approximately 95%, the acoustic emission b value of the weakly cemented sandstone appears to decrease rapidly. With an increase in the number of dry-wet cycles in the weakly cemented sandstone, the overall value of the b value increases, indicating that the proportion of small-scale damage increases during the failure process and that the softening effect of water on the weakly cemented rock is very obvious.

5.3. Characteristics of the Acoustic Emission Entropy of Weakly Cemented Sandstone under Dry-Wet Cycles. T. Clausius proposed the concept of entropy in 1854, and the size of entropy is related to the microscopic state of the system [37]. The microscopic state of the system is the thermodynamic probability that the system of a large number of mass points is obtained by statistical laws [38]: therefore, the entropy value is statistically significant. The essence of entropy is the degree of chaos inherent in a system. Therefore, the more uniform the energy distribution of a system is, the larger the entropy value is. This paper uses equation (9) to define the entropy value [39, 40]:

$$I(t) = -\sum_{n=1}^{N} P_n(t) \log P_n(t), \tag{9}$$

where I is the entropy value, N indicates the N level status of the system, and $P_n(t)$ is the probability of occurrence of this level of event. The entropy is normalized according to the following equation:

$$H(t) = I(t)/\log N, \tag{10}$$

where $H(t)$ is the normalized entropy value.

The entropy calculation process of weakly cemented rock under uniaxial compression failure under different dry-wet cycles is as follows. First, 1000 AE data are taken as a calculation period, and formula (7) is used to determine the acoustic emission magnitude M of this period. Second, the number of acoustic emissions of the same magnitude M in each set of data is calculated, and the probability of each magnitude M is calculated. Then, the entropy value is calculated according to formula (9), and finally the normalized entropy value is calculated by using formula (10). Finally, 100 acoustic emission events are used as the sliding window, and the end time of the window is used as the time to calculate the entropy value. The variation in the acoustic emission entropy value with time is obtained [41]. Therefore, the entropy value is a function of angle to measure the distribution of the magnitude of the emission and is one of the important parameters for measuring the level of acoustic emission activity.

According to the above method, the variation law of the acoustic emission entropy during the uniaxial compression failure of weakly cemented sandstone under different dry-wet cycles is obtained. The result is shown in Figure 15. The entropy curve fluctuates up and down during the uniaxial compression failure of weakly cemented sandstone. When the rock specimens of the dry-wet cycle at $N = 5$ and $N = 10$ are compared with the rock specimens of the dry-wet cycle at $N = 0$, the entropy value fluctuates at a low point during the initial stage, indicating that the acoustic emission event energy is small. When the weakly cemented sandstone is in the plastic stage, the acoustic emission entropy has a short-term reduction process, and the entropy mutation phenomenon is not obvious. It is considered that the crack propagates stably and the energy gathers. When the relative stress of the rock specimen reaches approximately 95%, the corresponding acoustic emission entropy value quickly reaches the maximum, and an entropy mutation occurs. The value indicates that many acoustic emission events are generated, the crack scale increases rapidly, and the weakly cemented sandstone undergoes unstable damage.

Figure 16 shows the curve of the overall magnitude of the acoustic emission entropy of the weakly cemented sandstone under different dry-wet cycles. The entropy value of the acoustic emission waveform signal is concentrated in the range of 0.1 to 0.6. With an increase in the number of dry-wet cycles, the acoustic emission entropy value decreases, and the acoustic emission event rate and energy release rate also decrease during the rock specimen failure process. The law of variation of the acoustic emission entropy is consistent with the results of Figure 12 but is exactly the opposite of the result of Figure 15. This finding indicates that the interaction between water and rock under the action of dry-wet cycles leads to significant weakening and deterioration of particulate matter and cementing materials in the weakly cemented sandstone.

The entropy value is a measure of the degree of chaos after a system is determined to be in a chaotic state and is a key indicator for the quantitative evaluation of the degree of stability of the system. If the entropy is small, then the system chaos is low, and if the entropy is large, then the system is chaotic. An increase in the entropy value indicates that the system evolves from a state with a small probability to a state with a high probability, that is, from a more regular and orderly state to a more irregular and more disordered state. With an increase in the number of dry-wet cycles, the fracture crack of the weakly cemented sandstone develops in the orderly direction of the local concentration, which reduces the entropy of the weakly cemented sandstone system. This result is consistent with the macroscopic crack characteristics of weakly cemented sandstone under different dry-wet cycles in Figure 7.

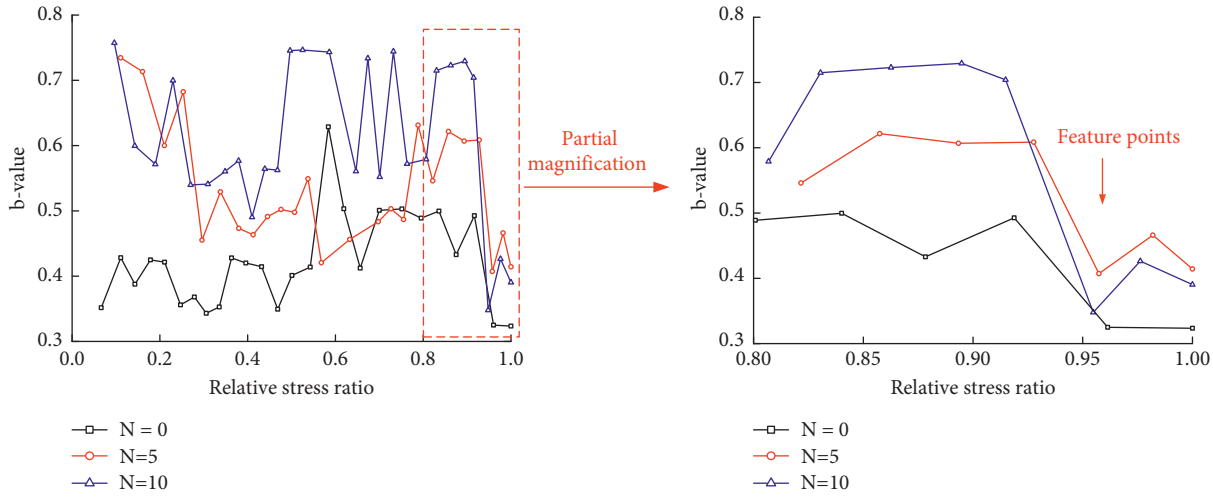

Figure 14: The change in the overall b value in the process of weakly cemented sandstone under different dry-wet cycles.

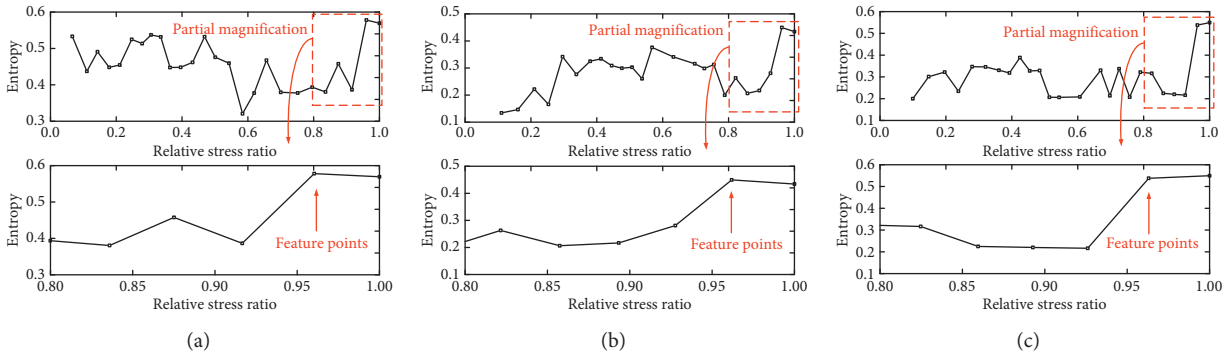

Figure 15: The variation rule of the acoustic emission entropy during the failure of weakly cemented sandstone under different dry-wet cycles. (a) $N = 0$. (b) $N = 5$. (c) $N = 10$.

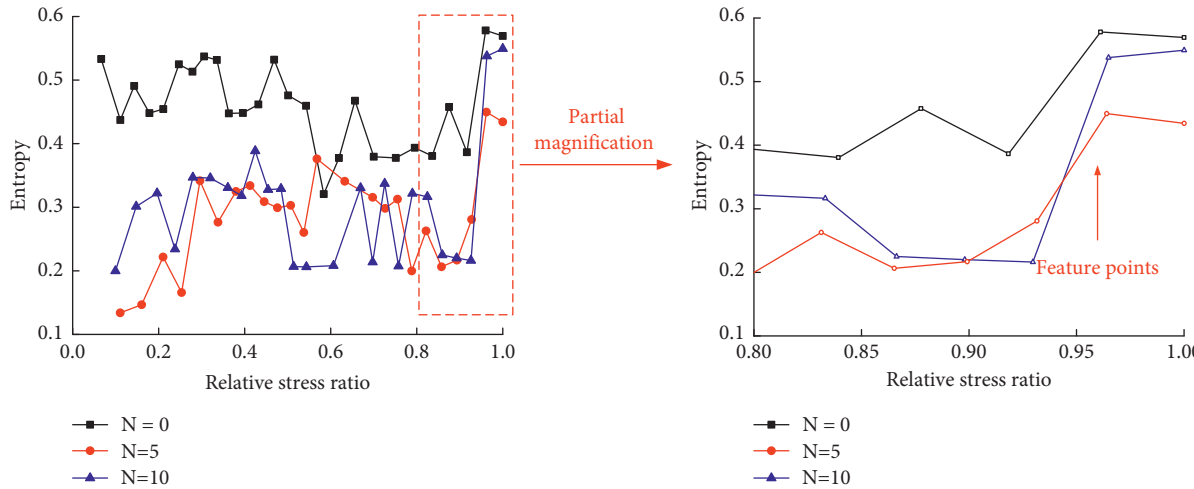

Figure 16: The change in the entropy value of the weakly cemented sandstone under different dry-wet cycles.

Table 2: Acoustic emission parameter information during the destruction of weakly cemented sandstone.

Acoustic emission parameters	Precursor feature	Number of dry-wet cycles	Corresponding critical relative stress value (%)	Comprehensive critical relative stress value (%)
Event rate	The event rate appeared to be close to 0 before the rupture, and then the platform oscillated, followed by a sudden rise.	$N = 0$	94	95
		$N = 5$	95.6	
		$N = 10$	95.5	
b value	The b value before the rupture suddenly drops, and the concentration range of the b value is 0.32~0.41.	$N = 0$	96	
		$N = 5$	95.3	
		$N = 10$	95.6	
Entropy	The entropy value rises before rupture, and the concentration interval of entropy is 0.47~0.58.	$N = 0$	96	
		$N = 5$	96.2	
		$N = 10$	96.7	

6. Coupling Criteria and Precursor Characteristics of Weakly Cemented Sandstone Specimen Fractures under Dry-Wet Cycles

Practice has shown that, for the prediction of rock failure, the differences among the same type of rock, microstructure, and mineral composition, as well as the diversity of influencing factors and disturbance factors in the rock failure process, are considered. A single information parameter to predict the critical damage precursor of rock has great limitations, cannot effectively identify the precursor information of rock disasters, and may have false positives or false negatives. Acoustic emission is an accompanying phenomenon of the rock failure process, and there is some corresponding relationship between the variation law of the characteristic parameters and stress evolution. Therefore, it is necessary to obtain the coupling characteristics between the rock stress and acoustic emission characteristic parameters and then to improve the accuracy and reliability of the critical damage precursor criterion.

By analyzing the variation characteristics of acoustic emission event rate, b value, and entropy value during the process of weakly cemented sandstone specimen rupture under different dry-wet cycles, the precursor information of the parameter mutation based on the acoustic emission is summarized. For weakly cemented sandstones under different numbers of dry-wet cycles, the absolute values of the same acoustic emission parameters are different, but the laws are consistent when the precursor rupture is reached. Therefore, the acoustic emission signal can reflect the essential characteristics of the fracture of the weakly cemented sandstone. Through the analysis of the data of Figures 12, 14, and 16, the results obtained are shown in Table 2.

Based on the above analysis, the acoustic emission signal, event rate, b value, and entropy value are suitable as the main parameters for the critical fracture prediction of weakly cemented sandstone. The acoustic emission signal event rate is an acoustic emission parameter that is sensitive to the lithology and rock structure. The b value and entropy of the acoustic emission signal can reflect the environmental characteristics of the weakly cemented sandstone and are acoustic emission parameters that are sensitive to the water content and stress state. When the weakly cemented sandstone reaches the critical failure state under different dry-wet cycles, the relative stress value is 95%.

7. Conclusion

(1) As the number of dry-wet cycles increases, the cemented material between the particles undergoes dissolution damage with respect to the microstructure, and the connectivity between the particles is enhanced. The interaction between water and rock causes cracks to occur, mainly in the cemented material; the water spreads along the boundaries of the particles, which changes the contact state between the particles. With an increase in the number of dry-wet cycles, the content of minerals such as quartz and mica in the weakly cemented sandstone increases, and the content of minerals such as potassium feldspar, albite, and illite decreases. The cemented material between the particles and the mineral particles themselves undergoes physical and chemical reactions, which generate a large amount of micropores and a local stress concentration on the microstructure, causing the particulate matter constituting the skeleton structure to peel off and the internal structural system to be destroyed, eventually leading to changes in the macroscopic physical and mechanical properties of the weakly cemented sandstones.

(2) As the number of cycles increases, the mass loss rate of the specimen increases first and then decreases, but the volume of weakly cemented sandstone does not change significantly. As the number of dry-wet cycles increases, the wave velocity loss rate gradually increases. Overall, the longitudinal wave loss rate is larger than the shear wave loss rate, indicating that the longitudinal wave is more sensitive to the degradation of weakly cemented sandstone.

(3) With an increase in the number of dry-wet cycles, the axial strain increases when the weakly cemented sandstone reaches the peak strength. The fracture crack is mainly caused by the main crack penetration

failure, and the secondary crack is significantly reduced. One reason is that the water dissolves some of the minerals in the weakly cemented sandstone under the action of dry-wet cycles, resulting in poor cementation performance between the particles; the other reason is that the process of water-rock interaction softens the existing particles and cement, resulting in a decrease in the stiffness of the microstructure system of the particles and the cement. The fractal dimension decreases with the rise of dry-wet cycles and reaches its maximum at 0 dry-wet cycles, which means that 0 dry-wet cycles witness the most complex morphology of fractures within the weakly cemented sandstone. This finding indicates that the dry-wet cycle inhibits the generation and expansion of fractures.

(4) For weakly cemented sandstones under different numbers of dry-wet cycles, the absolute values of the same acoustic emission parameters are different, but the laws are consistent when the precursor rupture is reached. Under the action of different dry-wet cycles, the acoustic emission event rate of weakly cemented sandstone is less during the initial stage, the elastoplastic phase increases slowly, and the peak stage reaches the maximum. The event rate appeared to be close to 0 before the rupture, and then the platform oscillated, followed by a sudden rise. The acoustic emission b value is relatively high in the initial stage and then decreases, which is the initial damage process; the elastoplastic phase rises again, the peak stage decreases rapidly, and the weakly cemented sandstone undergoes unstable damage. The change in the acoustic emission entropy value is exactly the opposite of the b value change law. When the weakly cemented sandstone reaches the critical failure state under different dry-wet cycles, the relative stress value is 95%.

(5) The multiparameter variation characteristics of acoustic emission during the process of weak cementation rock can reflect the degradation effect and influence the degree of water on its macroscopic strength and mesostructured materials. The test results provide new methods and a basis for the damage evolution mechanism and fracture prediction of the weakly cemented sandstone under dry-wet cycles. The acoustic emission monitoring and early warning of weak cemented sandstone damage in western China has important theoretical research significance.

Data Availability

The data used to support the findings of this study are included within the article.

Disclosure

A preprint has previously been published at the following link: https://www.sciencegate.app/keyword/613098.

Conflicts of Interest

The authors declare that they have no conflicts of interest.

Acknowledgments

This study was supported by the National Natural Science Foundation of China (Grant Nos. 52004125 and 52074100), the Key R&D project of Hebei Province, China (Grant no. 19275508D), and the Independence Technology Project of Beijing China Coal Mine Engineering Co. Ltd. (No. BMC-ZL-202004). The authors gratefully acknowledge this support.

References

[1] Z. Y. Song, H. G. Ji, H. Jiang, and Z. Liu, "Influence of wetting-drying cycles on acoustic emission characteristics and microstructure deterioration of weak cementation stratum," *Journal of China Coal Society*, vol. 43, no. S1, pp. 96–103, 2018.

[2] H. G. Ji, H. Jiang, Z. Y. Song et al., "Analysis on the microstructure evolution and fracture morphology during the softening process of weakly cemented sandstone," *Journal of China Coal Society*, vol. 43, no. 4, pp. 993–999, 2018.

[3] Q. B. Meng, L. J. Han, W. G. Qiao, D. G. Lin, and J. D. Fan, "Evolution of surrounding rock in pioneering roadway with very weakly cemented strata through monitoring and analysising," *Journal of China Coal Society*, vol. 38, no. 4, pp. 572–579, 2013.

[4] Z. Y. Song, H. G. Ji, Y. J. Liu, and L. Sun, "Influencing factors of excavation disturbance on neighboring roadways in weakly cemented rock," *J Min & Safety Eng*, vol. 33, no. 5, pp. 806–812, 2016.

[5] Q. B. Meng, L. J. Han, W. G. Qiao, and D. J. Lin, "Research on deformation failure characteristics of the deep high–stress soft rock roadways," *J Min & Safety Eng*, vol. 29, no. 4, pp. 481–486, 2012.

[6] W. S. Zhao, L. J. Han, Y. D. Zhang, Z. N. Zhao, and G. F. Wang, "Study on the influence of principal stress on the stability of surrounding rock in deep soft rock roadway," *J Min & Safety Eng*, vol. 32, no. 3, pp. 504–510, 2015.

[7] C. Y. Zhou, Y. M. Deng, X. S. Tan, Z. Q. Liu, and C. X. Lin, "Research on the variation regularities of microstructures in the testing of interaction between soft rocks and water," *Acta Scientiarum NaturaLium Univ Sun Yat-sen*, vol. 42, no. 4, pp. 98–102, 2003.

[8] Z. Y. Song, H. G. Ji, Z. Q. Liu, and L. Sun, "Study on the critical stress threshold of weakly cemented sandstone damage based on the renormalization group method," *Coal Science and Technology*, vol. 47, no. 4, pp. 101–106, 2020.

[9] C. Zhang, S. Jia, Q. Bai, H. Zhang, Y. Chen, and Y. Jiao, "CFD-DEM coupled simulation of broken rock mass movement during water seepage in an underground goaf reservoir," *Mine Water and the Environment*, vol. 40, pp. 1048–1060, 2021.

[10] S. Liu, G. S. Yang, and X. H. Dong, "Experimental study on influence of wetting-drying cycles on mechanical characteristics and damage of red sandstone," *Coal Science and Technology*, vol. 47, no. 4, pp. 101–106, 2019.

[11] Y. Fu, *Study on Water–Rock Interaction with the Cyclic Drying–Wetting Effect on Rock*, Chongqing University, Chongqing, China, 2010.

[12] H. Y. Yao, Z. H. Zhang, C. H. Zhu, Y. C. Shi, and Y. Li, "Experimental study of mechanical properties of sandstone

under cyclic drying and wetting," *Rock and Soil Mechanics*, vol. 12, p. 3704, 2010.

[13] H. Mei, Y. Zhu, and C. X. Niu, "Laboratory study on deterioration law of altered rock under effect of water saturation–dehydration circulation," *Journal of Engineering Geology*, vol. 23, no. 06, pp. 1039–1044, 2015.

[14] S. T. Qin, R. Liu, and X. H. Yang, "Experiment study of long–term stability of strongly weathered rock," *Central South Hydroelectric Engineering*, no. 2, pp. 41–48, 2006.

[15] H. F. Deng, J. L. Li, K. W. Wang, and J. Liu, "Research on secondary porosity changing law of sandstone under saturation–air drycycles," *Rock and Soil Mechanics*, vol. 33, no. 2, pp. 483–488, 2012.

[16] D. Ma, J. Zhang, H. Duan et al., "Reutilization of gangue wastes in underground backfilling mining : overburden aquifer protection," *Chemosphere*, vol. 264, Article ID 128400, 2021.

[17] P. A. Hale and A. Shakoor, "A laboratory investigation of the effects of cyclic heating and cooling,wetting and drying,and freezing and thawing on the compressive strength of selected sandstones," *Environmental and Engineering Geoscience*, vol. 9, no. 2, pp. 117–130, 2003.

[18] C. Apollaro, L. Marini, T. Critelli, and R. D. Rosa, "The standard themodynamic properties of vermiculites and prediction of their occurrence during water–rock interaction," *Applied Geochemistry*, vol. 35, pp. 264–278, 2013.

[19] M. Tallini, B. Parisse, M. Petitta, and M. Spizzico, "Long–term spatio–temporal hydro chemical and Rn–222 tracing to investigate groundwater flow and water–rock interaction in the Gran Sasso (central Italy) carbonate aquifer," *Hydrogeology Journal*, vol. 21, no. 7, pp. 1447–1467, 2013.

[20] P. A. Epping, L. W. Diamond, M. O. Haring, F. Lander, and D. B. Meier, "Prediction of water–rock interaction and porosity evolution in a granitoid–hosted enhanced geothermal system,using constraints from the 5 km Basel–1 well," *Applied Geochemistry*, vol. 38, pp. 121–133, 2013.

[21] J. A. Hurowitz and W. W. Fischer, "Contrasting styles of water–rock interaction at the Mars exploration rover landing sites," *Geochimica et Cosmochimica Acta*, vol. 127, pp. 25–38, 2014.

[22] C. W. Liu and S. L. Lu, "Research onmechanism of mudstone degradation and softening in water," *Rock and Soil Mechanics*, vol. 21, no. 3, pp. 28–31, 2000.

[23] H. W. Huang and P. Chen, "Research on micro–mechanism of softening and argillitization ofmudstone," *Journal of Tongji University:Natural Science*, vol. 35, no. 7, pp. 866–870, 2007.

[24] C. Y. Zhou, F. X. Zhu, and L. Zhang, "Research on saturation test and softening critical phenomena of soft rocks," *Rock and Soil Mechanics*, vol. 31, no. 6, pp. 1709–1715, 2010.

[25] J. Xu, H. Wu, and L. F. Lu, "Experimental study of acoustic emission characteristics during shearing of sandtone under different water contents," *Chinese Journal of Rock Mechanics and Engineering*, vol. 31, no. 5, pp. 914–920, 2012.

[26] D. Ma, J. J. Wang, X. T. Cai et al., "Effects of height/diameter ratio on failure and damage properties of granite under coupled bending and splitting deformation," *Engineering Fracture Mechanics*, vol. 220, Article ID 106640, 2019.

[27] H. T. Liu and T. Qin, "Study on damage characteristics and acoustic emission Kaiser effect of sandstone under cyclic loading and unloading conditions," *Coal Science and Technology*, vol. 47, no. 6, pp. 73–80, 2019.

[28] H. T. Wang, X. F. Xian, and J. M. He, "Triaxial mechanical properties of layered composite coal rocks," in *Ground Pressure and Strata Control*, no. 1, pp. 81–85, 1999.

[29] Y. Chen and L. Chen, *Fractal Geometry*, Earthquake Press, Beijing, China, 2005.

[30] Q. R. Meng, *Microscopic CT. Experimental Study on Pore and Fracture Evolution of Coal under Pyrolysis Condition*, Taiyuan University of Technology, Taiyuan, China, 2011.

[31] W. I. Friesen and R. J. Mikule, "Fractal dimension of coal particles," *Journal of Colloid and Interface Science*, vol. 20, no. 1, pp. 263–271, 1987.

[32] Z. G. Liang, R. He, Q. Chen, X. Xu, and J. Sato, "Fractal generation of char pores through random walk," *Combustion Science and Technology*, vol. 179, no. 3, pp. 637–661, 2007.

[33] H. Y. Li and Z. Y. Xu, "Microscopic characteristics of pore structure and classification evaluation of low permeability reservoir in Xinli oilfield," *Petrol. Geol Recov Effic*, vol. 16, no. 1, pp. 21–25, 2009.

[34] J. P. Zou, W. Z. Chen, D. S. Yang, H. Yu, and X. Tan, "The research of microstructure characteristics of Hunchun low–rank coal based on SEM," *Chinese Journal of Rock Mechanics and Engineering*, vol. 35, no. 9, pp. 1805–1814, 2016.

[35] B. Gutenberg and C. F. Richter, "Frequency of earthquakes in California," *Bulletin of the Seismological Society of America*, vol. 4, no. 4, pp. 185–188, 1944.

[36] L. M. Zhang, S. Q. Ma, M. Y. Ren, S. Jiang, Z. Wang, and J. Wang, "Acoustic emission frequency and b value characteristics in rock failure process under various confining pressures," *Rock and Soil Mechanics*, vol. 34, no. 10, pp. 2057–2063, 2015.

[37] C. E. Shannon, "A mathematical theory of communication," *Bell System Technical Journal*, vol. 27, no. 3, pp. 379–423, 1948.

[38] D. Harte, "The entropy score and its uses in earthquake forecasting," *Pure and Applied Geophysics*, vol. 162, pp. 1229–1253, 2005.

[39] L. H. Feng, "Maximum entropy principle and seismic magnitude–frequency relation," *Seismology and Geology*, vol. 25, no. 2, pp. 260–265, 2003.

[40] X. Z. Wang, C. S. Jiang, D. Q. Hong, and Z. M. Liu, "State analysis on strong earthquake activity in West China continent based on seismic information entropy of weibull distribution," *Earthquake*, vol. 31, no. 1, pp. 58–65, 2011.

[41] J. L. Wei, S. J. Liu, L. X. Wu, J. Huang, Y. Zhang, and B. Tian, "Comparative analysis on different AE parameters in biaxial loading of hole rock," *Journal of Mining & Safety Engineering*, vol. 32, no. 06, pp. 1017–1025, 2015.